Real-time modeling of optical orientation in GaAs: Generation and decay of the degree of spin polarization

M. D'Alessandro[1] and D. Sangalli[2]
[1]*Division of Ultrafast Processes in Materials (FLASHit), Istituto di Struttura della Materia-CNR, Via del Fosso del Cavaliere 100, 00133 Rome, Italy*
[2]*Division of Ultrafast Processes in Materials (FLASHit), Istituto di Struttura della Materia-CNR, Area della Ricerca di Roma 1, Monterotondo Scalo, Italy*

(Received 12 June 2020; revised 15 September 2020; accepted 15 September 2020; published 30 September 2020)

We present a real-time *ab initio* description of optical orientation in bulk GaAs due to the coupling with an ultrashort circularly polarized laser source. The injection of spin-polarized electrons in the conduction band is correctly reproduced, and a nonvanishing spin polarization **P** parallel to the direction of propagation of the laser (z) emerges. A detailed analysis of the generation and the evolution of $\mathbf{P}(t)$ is given. The single **k**-point dynamics is a motion of precession around a fixed axis with constant $|\mathbf{P}|$ and fixed frequency. Instead, the **k**-integrated signal shows only a time-dependent $P_z(t)$ and decays a few picoseconds after the end of the laser pump due to decoherence. Decoherence emerges since the individual contributions activated by the pump give rise to destructive interference. We interpret the results in terms of the *free induction decay* mechanism proposed some years ago [M. W. Wu and C. Z. Ning, Eur. Phys. J. B **18**, 373 (2000)]. We are able to reproduce such an effect in a full *ab initio* fashion, giving a quantitative estimate of the associated decay time. Our result also shows a possible explanation for the time decay of spin magnetization observed in many real-time *ab initio* simulations.

DOI: 10.1103/PhysRevB.102.104437

I. INTRODUCTION

The control of the spin degree of freedom by optical means is the key to the realization of ultrafast magnetic devices, where the reading and writing of information could be performed on the femtosecond timescale. That is why, following the first experimental demonstration of ultrafast optical demagnetization in nickel [1], very rich activity, both experimental and theoretical, started with the emerging of a new research area called femtomagnetism [2]. Different physical effects are involved in the indirect interaction between spin and light, and in all of them, spin-orbit coupling (SOC) plays a crucial role [3]. While most of the studies focus on magnetic or antiferromagnetic materials, the control of the spin degree of freedom can be achieved in paramagnetic materials via circularly polarized light. An example is optical orientation [4–6] in GaAs due to the interplay between SOC and the space group of the crystal which determines the selection rules for light absorption at the Γ point of the Brillouin zone (BZ). If GaAs is excited with a circularly polarized laser pulse whose frequency is tuned close to the optical gap, an imbalance between the spin-up and the spin-down electronic densities in the conduction band is generated. Such an effect was known [7] long before the realization of the first ultrafast experiment on the femtosecond timescale, and it was studied, in particular, in GaAs quantum wells [8]. It already has technological interest on its own for the generation of spin-polarized currents for spintronics devices. The underlying physics can be captured by a simple six-state model [7,9–11] (eight states are needed if the split-off bands need to be included). The degree of polarization predicted by the model in the conduction band is 50%, in good agreement with experimental results [6]. The few-state model has the advantage of clearly capturing the physics of optical orientation, giving a simple interpretation in terms of populations in the different bands of GaAs. A description beyond such a simple model can be achieved via the $\mathbf{k}\cdot\mathbf{p}$ approach, which also describes how the degree of spin polarization changes moving away from the Γ point, i.e., tuning the laser frequency above the optical gap value. A fully *ab initio* description was formulated more recently [12], studying the second-order response derived from the equation of motion for the density matrix. The approach of Ref. [12] highlighted the role played by coherences between SOC spin-split bands in the conduction. The SOC spin splitting is due to the lack of inversion symmetry in GaAs and exists only if band dispersion away from the high-symmetry lines is considered. Coherences between such spin-split bands account for ≈70% of the spin polarization induced by the optical pulse.

While these works clarified the physics behind optical orientation, they remained confined to the description in frequency space. In view of the renewed interest in spin and spin currents for femtomagnetism applications [13,14], an approach in the time domain is instead needed. In this work we adopt a fully *ab initio* real-time approach, and we show that it captures the correct value of the degree of spin polarization in the conduction band (and also in the valence band). We are able to follow its coherent generation and predict that the superimposed dynamics of the coherences are responsible for a subsequent decay on a timescale of a few picoseconds.

In the time domain the key question is, indeed, how the spin polarization evolves and decays [15,16]. The *ab initio* realization of real-time spin dynamics is a new and very

exciting approach which has seen renewed interest in recent years [17–19] for the possibility to shine new light on such key questions. However, the connection between these recent works and the broad and well-established literature of spin relaxation models and mechanisms [20–25] is not always clear. The two most established spin decay channels [3] are the Dyakonov-Perel (DP) and the Elliott-Yaffet (EY) mechanisms, which are both related to the interplay between SOC and scattering. The dynamics due to the DP mechanism is dictated by the ratio between the spin precession time $1/\Omega$, i.e., the characteristic time frequencies of the coherences in our language, and the scattering time τ_p. In the weak-scattering regime, $\Omega\tau_p > 1$, spin precession leads to *free induction decay* in the presence of a continuous distribution of frequencies (*inhomogeneous broadening*) [3,26,27]. We will interpret our results while taking advantage of these concepts to put a bridge between the *ab initio* community and the physics of models.

Let us remark that, as already discussed in the literature [12], a critical aspect in the description of optical properties in GaAs is the k sampling of the BZ. In this work we adopt a specific ultrafine sampling of random points around the Γ point. The size of the region is chosen according to the frequency profile of the laser pulse used in the real-time propagation.

II. OPTICAL ORIENTATION

The time-dependent magnetization of optically excited electrons in the conduction band can be probed in time-resolved photoemission (PE) experiments. In the present case GaAs is driven out of equilibrium by a femtosecond circularly polarized laser pulse, with the pump, whose frequency is tuned to 1.5 eV, slightly above the direct gap of GaAs. To fix the geometry we define z as the direction of propagation of the field, which is then circularly polarized in the x-y plane. We consider a pulse whose envelope is a Gaussian function with a FWHM of 100 fs. This corresponds to an energy spread of the pulse of around 40 meV.

Since spin is a one-body operator, the dynamics of the "degree of spin polarization" for electrons excited in the conduction band $P_z^c(t)$ can be expressed in terms of the time-dependent one-body reduced density matrix (DM) $\hat{\rho}(t)$ as follows:

$$P_z^c(t) = \frac{\mathrm{tr}[\hat{\rho}^c(t)\hat{S}^z]}{\mathrm{tr}[\hat{\rho}^c(t)]}. \tag{1}$$

Here $\hat{S}_z$ is the z component of the spin operator, and $\hat{\rho}^c(t) = \hat{\Pi}_c\hat{\rho}(t)\hat{\Pi}_c$ is the projection of the nonequilibrium density matrix in the conduction subspace via the projector $\hat{\Pi}_c$. Equation (1) can be obtained from the definition of the PE signal, assuming a probe pulse longer than the very fast oscillations of $\hat{\rho}$ in the $\{cv\}$ channel and enough energy to extract electrons only from the conduction band. We observe that P_z^c defined according to Eq. (1) is an intensive quantity that measures the ratio between the expectation value of the spin operator, restricted in the conduction subspace, and the number of carriers.

The time dependence of Eq. (1) is codified in the equation of motion (EOM) for $\hat{\rho}(t)$, which can be derived from the Kadanoff-Baym equation under the generalized Kadanoff-Baym approximation. We express $\hat{\rho}(t)$ in the basis of the Kohn-Sham (KS) states

$$\hat{\rho} = \sum_{nm\mathbf{k}} \rho_{nm\mathbf{k}} \, |n\mathbf{k}\rangle \, \langle m\mathbf{k}| \, , \tag{2}$$

where the band indices n, m run over the KS states, both occupied and empty, and $\mathbf{k}$ is the Bloch momentum. The EOM for matrix elements of $\hat{\rho}(t)$ in the KS basis can be expressed as

$$i\partial_t \rho_l = \epsilon_l \rho_l + [\Delta\hat{\Sigma}[\hat{\rho}], \hat{\rho}]_l + [\hat{U}^{\mathrm{pump}}, \hat{\rho}]_l + S_l[\hat{\rho}], \tag{3}$$

where $l = \{nm\mathbf{k}\}$ is a compact multi-index notation and $[\hat{O}, \hat{\rho}]_l$ is the matrix element of the commutator between the operator $\hat{O}$ and the DM expressed in the KS basis. $\hat{U}^{\mathrm{pump}}$ describes the pump pulse, i.e., the source term that drives the system out of equilibrium. $\Delta\hat{\Sigma}[\hat{\rho}]$ is the self-consistent variation of the static part of the self-energy, including the mean field, while $\hat{S}[\hat{\rho}]$ captures the variation in the dynamical part of the self-energy, including possible dissipation and relaxation effects.

In the present analysis we work with time-dependent independent particles (TD-IPs); thus, $\Delta\hat{\Sigma}[\hat{\rho}] = 0$. We also neglect all dynamical many-body effects and simplify the scattering term to a damping in the $\{cv\}$ channel: $S_{nm\mathbf{k}}[\hat{\rho}] = -\eta_{cv}|f^{eq}_{n\mathbf{k}} - f^{eq}_{m\mathbf{k}}|\rho_{nm\mathbf{k}}$. This term is needed to *cure* the finite nature of the BZ sampling and to provide converged results (further details on its choice are discussed in the next sections). Instead, no decoherence term is imposed in the $\{cc\}$ channel, and accordingly, P_z^c defined in Eq. (1) fully contains the coherent signal.

Equation (3) has been solved in the time domain by using a development version of the YAMBO package [28,29] that evaluates the temporal evolution of $\rho_l(t)$ through a second-order Runge-Kutta integrator. The resulting P_z^c computed propagating equation (3) on a fine random grid centered around the Γ point is shown in Fig. 1. Details of the simulations are discussed in the next sections. A value for P_z^c very close to the theoretical result $P_z^{c,\mathrm{theo}} = 0.5$ is reproduced as soon as the laser is switched on (it takes just a few femtoseconds, i.e., about an optical cycle of the laser; see the inset). The small

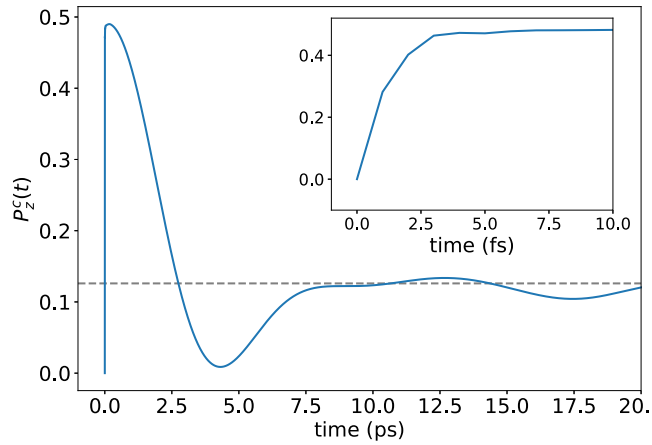

FIG. 1. Degree of spin polarization as a function of time. The horizontal dashed line represents the noncoherent contribution due to only the populations, i.e., considering only the diagonal elements of the density matrix.

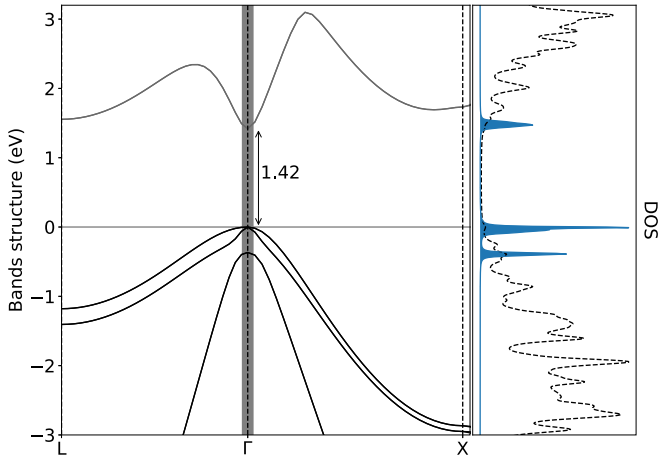

FIG. 2. Left: Band structure including the scissor correction along the L-Γ-X path. The shaded gray slice close to Γ denotes the $\mathbf{K}_{\text{pump}}$ optical active region. Right: The black dashed curve represents the DOS of the system. The blue shaded area shows the DOS restricted to the $\mathbf{k}$ points in the optical active region. The two curves are rescaled for better visualization.

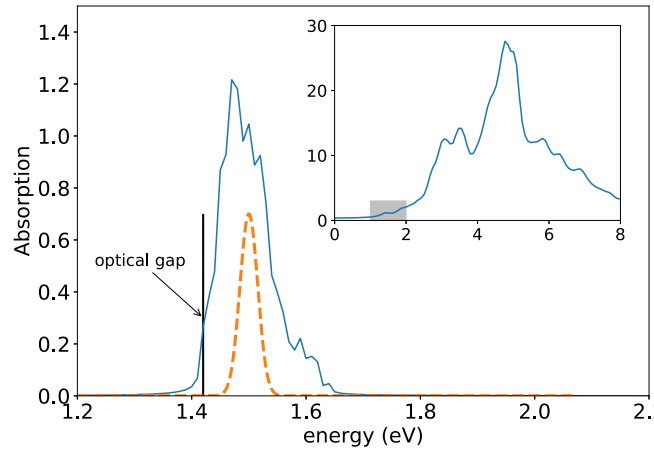

FIG. 3. The blue line shows absorption from the top of the valence bands due to transitions from the heavy/light holes to the lower conduction bands. The orange dashed line describes the energy profile of the pump, centered at 1.5 eV. The inset shows the absorption associated with all the allowed transitions in a wider energy range. The gray shaded area of the inset is the part of the spectrum represented in the main frame.

discrepancy with respect to the results of the simple model [7] at Γ is easily understood since the real-time pump, due to its energy and finite temporal width, activates also transitions aside from Γ, where the ratio between spin-up and spin-down transitions is not exactly 3:1. $P_z^c(t)$, however, drops on the timescale of a few picoseconds, even though no decoherence mechanism is included in the EOM for the cc channel. Indeed, the coherent contribution drops to zero due to the free induction decay, despite all $\rho_{cc'\mathbf{k}}(t)$ terms remaining finite and oscillating in time at $\Delta\epsilon_{cc'\mathbf{k}}$. We refer to the residual spin polarization $P_z^c(\infty)$ as a "dephased limit." $P_z^c(\infty) \approx P_z^{c,\text{diag}}$, the value obtained imposing $\rho_{cc'\mathbf{k}} = 0$ if $c \neq c'$. $P_z^{c,\text{diag}} \approx 0.125$ is less than 30% of $P_z^{c,\text{theo}}$, as predicted in the literature [12], and is marked by the horizontal dashed line in the plot.

A. Preliminary analysis of the band structure

KS energies and wave functions are computed with a noncollinear approach and using the Perdew-Burke-Ernzerhof (PBE) [30] exchange and correlation functional, as implemented in the QUANTUM ESPRESSO package [31,32]. SOC is included via fully relativistic pseudopotentials for both Ga and As. The ground state of the system is obtained with the following convergence parameters: a $6 \times 6 \times 6$ Monkhorst-Pack $\mathbf{k}$ grid and an energy cutoff of 80 Ry that ensure convergence in the total energy at the level of a fraction of 1 meV. The equilibrium lattice constant for the given description of the GaAs lattice was computed by relaxing the system. The lattice parameter that provides a stable configuration is $a_{\text{lat}} = 5.54$ Å. Empty bands are evaluated by performing non-self-consistent computations based on the converged density. As expected, PBE underestimates the (direct) band gap, and we have improved the density functional theory (DFT) band structure using the *scissor operator* [33–35]. A value of 0.55 eV is chosen to match the "experimental" band gap of 1.42 eV at 300 K. The corrected band structure along the L-Γ-X high-symmetry path is shown in Fig. 2. Along such a path each band is twofold degenerate and can accommodate both "spin-up" and "spin-down" electrons. In the valence sector we recognize the heavy and light holes, together with the split-off bands lifted down by the SOC.

In view of the solution of Eq. (3) we need a fine sampling which includes the *optical active region* of the BZ, i.e., all the transitions $\Delta\epsilon_{cv\mathbf{k}} \approx \omega_0 \pm \Delta_0$ that can be activated by the pump. Given the frequency profile of the pump pulse, we chose a cube, denoted as $\mathbf{K}_{\text{pump}}$, with an edge of 0.05 (in units of $2\pi/a_{\text{lat}}$) centered at Γ. $\mathbf{K}_{\text{pump}}$ is highlighted in Fig. 2 with gray shading, and it is sampled with $N_k = 24\,000$ points, generated expanding by symmetry an initial set of 500 random points with a uniform distribution. The symmetry expansion is needed since only a specific portion of the BZ is activated by the pump pulse and to avoid spurious symmetry breaking in the simulations. All 24 000 points lie within $\mathbf{K}_{\text{pump}}$, and $\rho_{nm\mathbf{k}}(t)$ is defined and propagated for each of them. If the whole BZ had been sampled with the same density, 4.8×10^7 $\mathbf{k}$ points would have been needed. To understand why such a fine sampling is needed, the absorption $\text{Im}[\epsilon(\omega)]$ from the light and heavy hole states to the first conduction within $\mathbf{K}_{\text{pump}}$ is shown in Fig. 3 and compared with the frequency profile of the laser pulse. $\text{Im}[\epsilon(\omega)]$ can be obtained from the Fourier transform of the polarization, $\mathbf{P}(t) = \sum_{cv\mathbf{k}} \mathbf{x}_{cv\mathbf{k}} \rho_{cv\mathbf{k}}(t)$. In order to overcome unphysical δ-shaped structures due to the finite nature of the sampling and to ensure that the pump pulse is correctly absorbed, the $\rho_{cv\mathbf{k}}(t)$ matrix elements are dephased by a parameter η_{cv}, which transforms each peak into a Lorentzian function. Due to the nominal width of the laser pulse of 40 meV, we set $\eta_{cv} = 4$ meV. The reason for this choice is a balance between faster convergence (bigger η) and letting the spread of the optically activated $\mathbf{k}$ region be determined by the laser pulse. Figure 3 highlights that the chosen sampling and the size of $\mathbf{K}_{\text{pump}}$ are adequate. In Fig. 3 we also show that the pump is tuned 80 meV above the optical gap.

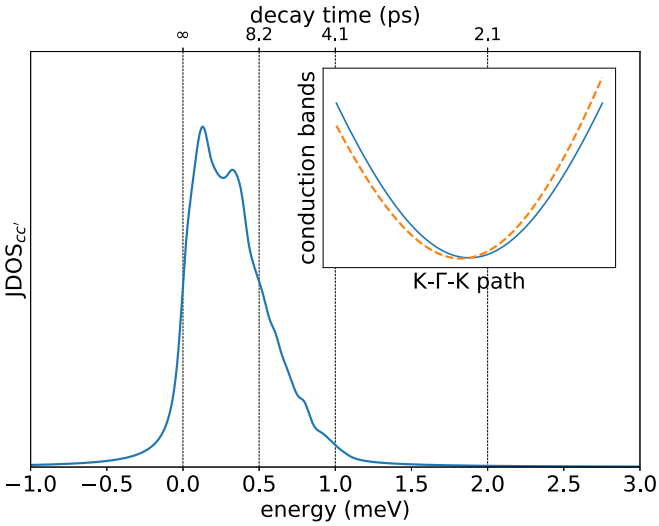

FIG. 4. JDOS$_{cc'}$ of the direct transitions between the spin-split states of the conduction bands. The inset contains a representation of the conduction bands along the K-Γ-K path close to the Γ point.

Although the first two conduction bands are degenerate along the L-Γ-X path (see Fig. 2), this is not the case for other $\mathbf{k}$ points in the $\mathbf{K}_{\text{pump}}$ region. A detailed analysis [36] shows that the SOC, together with the lack of inversion symmetry, is responsible for a spin splitting away from the high-symmetry lines, with $\epsilon_{\uparrow\mathbf{k}} \neq \epsilon_{\downarrow-\mathbf{k}}$ (see the inset of Fig. 4). Let us now focus on such transitions in the conduction sector that will determine the dynamics of $\rho_{cc'\mathbf{k}}(t)$. The joint density of states in this sector (JDOS$_{cc'}$) is reported in Fig. 4. The energy differences $\Delta\epsilon_{cc'\mathbf{k}} \approx (\epsilon_{\uparrow\mathbf{k}} - \epsilon_{\downarrow\mathbf{k}})$ in the $\mathbf{K}_{\text{pump}}$ region are of the order of a few tenths of a meV and limited to a maximum energy of 1 meV. We thus expect a dynamics on the picosecond timescale associated with such energy differences (1 meV $\rightarrow$ 4 ps; see the upper x axis in Fig. 4). Also in this case we need to choose a spread parameter η_{cc} in this channel to balance between faster convergence (big η_{cc} and smoother JDOS$_{cc'}$) and avoiding altering the dynamics on the picosecond timescale. We use the value $\eta_{cc} = 0.05$ meV($\rightarrow$ 80 ps), which is about a factor of 10 smaller than what would impact the results of our real-time simulations but big enough to have a smooth JDOS$_{cc'}$.

B. Real-time simulations

The degree of spin polarization P^c_z, Eq. (1), can be expressed explicitly in the KS basis, using $\hat{\Pi}_c = \sum_{c\mathbf{k}} |c\mathbf{k}\rangle \langle c\mathbf{k}|$:

$$P^c_z(t) = \frac{\sum_{cc'\mathbf{k}} \rho_{cc'\mathbf{k}}(t) S^z_{c'c\mathbf{k}}}{\sum_{c\mathbf{k}} \rho_{cc\mathbf{k}}(t)}, \tag{4}$$

where

$$S^z_{cc'\mathbf{k}} = \frac{1}{2} \int d\mathbf{r} [\psi^*_{c\mathbf{k}\uparrow}(\mathbf{r}) \psi_{c'\mathbf{k}\uparrow}(\mathbf{r}) - \psi^*_{c\mathbf{k}\downarrow}(\mathbf{r}) \psi_{c'\mathbf{k}\downarrow}(\mathbf{r})].$$

By considering the coupling with the pump of the form of a dipole interaction, i.e., $U^{\text{pump}}(t) = \mathbf{E}(t) \cdot \mathbf{r}$, we can recast Eq. (3) as a damped oscillatory equation driven by a self-consistent source,

$$\partial_t \rho_l + i\Omega_l \rho_l = F_l[\rho], \tag{5}$$

where $\Omega_l = \epsilon_l - i\eta_l$ and η_l is the dephasing parameter presented in Sec. II A: $\eta_l = \eta_{cv} = 4$ meV in the $\{cv\}$ channel and $\eta_l = \eta_{cc} = 0.05$ meV in the $\{cc'\}$ one. The source term of Eq. (5) reads

$$F_{nm\mathbf{k}}[\rho] = -i\mathbf{E}(t) \cdot \sum_p (\mathbf{d}_{np\mathbf{k}} \rho_{pm\mathbf{k}} - \rho_{np\mathbf{k}} \mathbf{d}_{pm\mathbf{k}}), \tag{6}$$

where $\mathbf{d}_l$ are the matrix elements of the dipole operator in the KS basis. Expanding the DM in powers of the pump, up to the two-photon term, we obtain

$$\rho_{nm\mathbf{k}}(t) = \delta_{nm} f^{eq}_{n\mathbf{k}} + \rho^{(1)}_{nm\mathbf{k}}(t) + \rho^{(2)}_{nm\mathbf{k}}(t) + \cdots.$$

For times preceding the activation of the pump we have set $\rho_{nm\mathbf{k}} = \delta_{nm} f^{eq}_{n\mathbf{k}}$, so that the DM is defined by the equilibrium occupations of states. Plugging this expansion into Eqs. (5) and (6) provides a chain of differential equations for $\rho^{(i)}_l$:

$$\partial_t \rho^{(i)}_{nm\mathbf{k}} + i\Omega_{nm\mathbf{k}} \rho^{(i)}_{nm\mathbf{k}} = F^{(i)}_{nm\mathbf{k}}, \tag{7}$$

which can be hierarchically solved starting from the lowest order. At the one-photon level the source term reads

$$F^{(0)}_{nm\mathbf{k}} = -i\big(f^{eq}_{n\mathbf{k}} - f^{eq}_{m\mathbf{k}}\big)\mathbf{E}(t) \cdot \mathbf{d}_{nm\mathbf{k}}$$

and is not vanishing only for transitions between valence and conduction states. The solution of Eq. (7) at a one-photon level shows that only the matrix elements $\rho^{(1)}_{cv\mathbf{k}}$ with $\Delta\epsilon_{cv\mathbf{k}} \sim \omega_{\text{pump}}$ are activated by the pump through a resonance mechanism. After an initial transient regime, these terms exhibit an oscillatory behavior suppressed by an exponential factor, i.e., $\exp[-i(\Delta\epsilon_{cv\mathbf{k}} - i\eta_{cv\mathbf{k}})t]$.

Going ahead in the hierarchy of Eq. (7), the $\rho^{(2)}_{nm\mathbf{k}}$ terms are activated by two-photon processes. Here we are interested in the generation of $\rho^{(2)}_{cc'\mathbf{k}}$, which are leading terms in the cc' channel. The source term associated with transitions among conduction states reads

$$F^{(2)}_{cc'\mathbf{k}} = -i\mathbf{E}(t) \cdot \sum_v \big[\mathbf{d}_{cv\mathbf{k}} \rho^{(1)}_{vc'\mathbf{k}} - \rho^{(1)}_{cv\mathbf{k}} \mathbf{d}_{vc'\mathbf{k}}\big]. \tag{8}$$

The $\rho^{(2)}_{cc'\mathbf{k}}$ terms are activated when both $\Delta\epsilon_{cv\mathbf{k}}$ and $\Delta\epsilon_{c'v\mathbf{k}}$ lie within $\omega_0 - \Delta_0$ and $\omega_0 + \Delta_0$. Under this condition, $F^{(2)}_{cc'\mathbf{k}}$ contains *fast* oscillating terms modulated by an envelope with frequency $\Delta\epsilon_{cv\mathbf{k}} - \Delta\epsilon_{c'v\mathbf{k}}$ which couples resonantly with the transitions $\Delta\epsilon_{cc'\mathbf{k}}$, activating a *slow* oscillatory response of the system on the picosecond timescale. We now inspect the terms for which $S^z_{cc'\mathbf{k}}$ is maximum. For $c = c'$, maximum $S^z_{cc\mathbf{k}}$ occurs when $\hat{S}^z \psi_{c\mathbf{k}} \approx \pm 1/2 \psi_{c\mathbf{k}}$, i.e., for eigenstates of $\hat{S}^z$. Instead, for $c \neq c'$, $S^z_{cc'\mathbf{k}}$ is maximum for $\hat{S}^z \psi_{c\mathbf{k}} \propto \psi_{c'\mathbf{k}}$. Since $\psi_{c\mathbf{k}}$ and $\psi_{c'\mathbf{k}}$ have opposite spin directions, the latter condition is satisfied for eigenstates of $\hat{S}^x$ or $\hat{S}^y$. Notice that at Γ, and, more generally, whenever $\Delta\epsilon_{cc'\mathbf{k}} = 0$, one can choose an arbitrary rotation in the degenerate space so that only the diagonal terms survive. Then everything is described in terms of eigenstates of $\hat{S}^z$, as in the standard interpretation of the six-state model [7,9]. When $\Delta\epsilon_{cc'\mathbf{k}} > 0$, this is not possible anymore, and other states (including eigenstates of $\hat{S}^x$ or $\hat{S}^y$) must be involved.

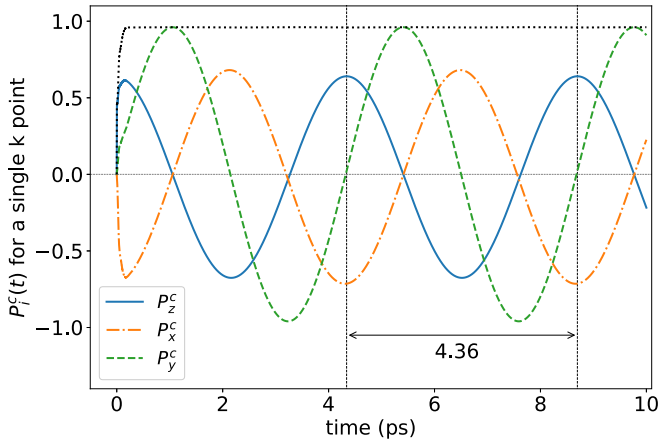

FIG. 5. Time profile of the components of the degree of spin polarization associated with a single **k** point, denoted $\mathbf{k}_M$ in the text, with Cartesian coordinates $[-0.025, 0.0076, 0.024]$ in units of $2\pi/a_{\text{lat}}$. The orange dot-dashed, green dashed, and blue solid lines show the time behavior of the x, y, and z components, respectively. The black dotted line represents the time profile of the modulus of $\mathbf{P}^c(t)$. All the components $P_i^c(t)$ oscillate with the same frequency of 4.36 ps, as shown.

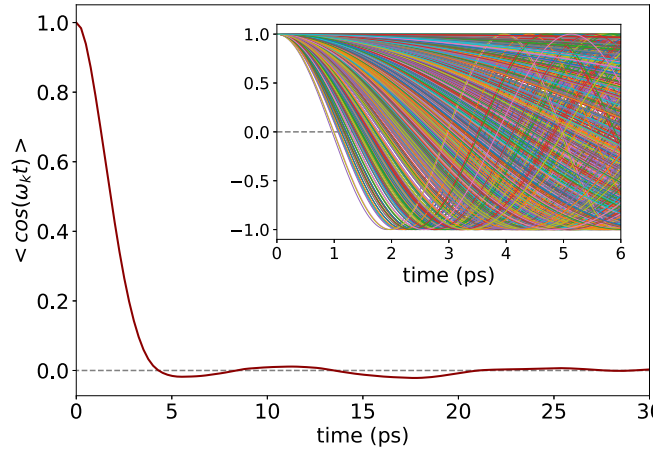

FIG. 6. Time profile of the average of oscillating functions with frequencies equal to the difference of the spin-split conduction bands. The inset shows the profiles of the various addends.

In order to provide numerical support to these analytical considerations we have performed a real-time calculation including a single **k** point. For this test we have selected the point $\mathbf{k}_M$ for which the transition energy between $\Delta\epsilon_{cc'\mathbf{k}} =$ 0.948 meV is the maximum, among the points sampled in the $\mathbf{K}_{\text{pump}}$ region. In Fig. 5 we plot the contribution of such a point to $P_i^c(t)$, with $i = \{x, y, z\}$. After a transient regime of the temporal range of the cycle of the pump, the three components $P_i^c(t)$ oscillate with a frequency that exactly matches the energy difference of the spin-split conduction bands (0.948 meV $\rightarrow$ 4.36 ps). The black dotted line shows that $P^c = \sqrt{\sum_i (P_i^c)^2}$ remains constant during the time evolution. Moreover, we have verified that, if the contributions of all the points connected to $\mathbf{k}_M$ by the symmetry are considered, then $P_x^c = P_y^c = 0$, while $P_z^c(t)$ keeps the same oscillatory behavior reported by the blue curve in Fig. 5. Thus, while the single-**k** dynamics is captured by a precession around a fixed axis, including symmetries, the global dynamics results in a time oscillation in the modulus of $\mathbf{P}^c$. This can be visualized in the simplified case with two **k** points, and

$$\mathbf{P}^c(\mathbf{k}_1) = P^c(0, +\cos(\omega t), \sin(\omega t)),$$
$$\mathbf{P}^c(\mathbf{k}_2) = P^c(0, -\cos(\omega t), \sin(\omega t)).$$

C. Superposition of all k points: Emergence of a dephasing time

We now turn to the global dynamics which results from the sum over the dense sampling of the single-**k** dynamics discussed in the previous section. As shown in Fig. 1, the expectation value of $P_z^c(t)$ decays on the timescale of a few picoseconds after the end of the pump. This behavior emerges despite the fact that no dephasing mechanisms are present at this timescale and is due to the destructive interference among the elements of the spin ensemble in the $\mathbf{K}_{\text{pump}}$ region which are actually activated by the pump pulse.

We further inspect this mechanism through a numerical test. P_z^c is the integral over **k** of terms which oscillate as $\cos(\omega_{\mathbf{k}} t)$, as shown in Fig. 5. In Eq. (4) the integral is performed as a simple sum. Here, instead, neglecting that each contribution has a different amplitude, we carefully perform $\int d\omega \cos(\omega t) j(\omega)$, where $j(\omega)$ is the $\text{JDOS}_{cc'}$ of Fig. 4. To this end we use a trapezium method on a dense mesh of frequencies interpolated from the initial 500 $\Delta\epsilon_{cc'\mathbf{k}}$ *ab initio* energies. The result is shown in the main frame of Fig. 6. It has a time profile very similar to that of $P_z^c(t)$ in Fig. 1, with complete decoherence taking place in $\approx$4 ps, as a consequence of the Riemann-Lebesgue lemma.

Last, we observe that this numerical test allows us to identify the residual long-time oscillations of Fig. 1 due to the finite number of **k** points used to build P_z^c in the real-time approach. Indeed, for a finite ensemble a finite portion of spin can be partially in phase after some time (revival of Rabi oscillations), whereas in the continuum limit the amplitude of the long-time oscillations vanishes since the revival time goes to infinity.

III. DISCUSSION AND CONCLUSIONS

We have proven that the dynamics of the degree of spin polarization, under the action of an ultrashort laser pulse, can be fully captured within an *ab initio* approach. The analysis of the single **k**-point dynamics shows that a spin precession mechanism is activated. Such precession is determined by the local magnetic field connected to the magnitude and the direction of the SOC at such **k**, as in standard Bloch models for spin dynamics [3,27]. The spin polarization oscillates between S_z, S_x, and S_y. In the superimposed dynamics of the symmetry-connected **k** points, which takes into account the symmetries of the lattice external potential, the x and y components of the spin polarization sum to zero at any time. Thus, the spin precession turns into a periodic transfer of angular momentum from kinetic to potential rotational energy. Only by breaking such symmetries, for example, via the use of an external magnetic field, would the spin precession ap-

pear in the macroscopic analysis. The understanding of this mechanism gives a key instrument to interpret recent works on spin dynamics based on time-dependent DFT in magnetic materials [17–19], where, similarly, only the z component of the magnetization evolves in time.

The overall dynamics, due to the collective response of the system, experiences a decoherence process on the timescale of a few picoseconds due to the superimposed dynamics of periodic functions with multiple frequencies $\Delta\epsilon_{cc'\mathbf{k}}$. In the literature such a process is named the free induction decay mechanism [3,22]. Following standard notation, we refer to the global dephasing times as longitudinal (T_1^*) and transverse (T_2^*). In the absence of external magnetic fields $T_1^* = T_2^*$. Moreover, we have $1/T_2^* = 1/T_2 + 1/T_2'$, where T_2 accounts for explicit dephasing processes, which are negligible in our simulations, while T_2' accounts for the free induction decay mechanism, which we measure in the present work. In order to obtain reliable results we have chosen very small values of the dephasing parameters η_{cv} and η_{cc} to be sure that they do not affect the dynamics of the system on the temporal scale of the free induction decay time. Following this choice, the numerical convergence has been carefully checked via the use of a very fine sampling of the $\mathbf{k}$ space in the optical active region. This approach enables us to obtain a full ab initio evaluation of T_2'. It provides an important alternative to better understand such a mechanism and gives a quantitative numerical calculation of its impact. Given the chosen parameters for the pump pulse, T_2' depends on the JDOS$_{cc'}$ of GaAs $\Delta\epsilon_{cc'\mathbf{k}}$ in the subset of $\mathbf{k}$ points activated by the pump. Such a subset contains all points for which $\Delta\epsilon_{cv\mathbf{k}} \approx \omega_0 \pm \Delta_0$. We used a pump pulse detuned by 80 meV from the optical gap of GaAs, $(\omega_0 - \Delta\epsilon_{cv\mathbf{0}}) \approx 80$ meV, as shown in Fig. 3, and found that such detuning, rather than the value of Δ_0, determines the decoherence time under such conditions. Indeed, even in the limit $\Delta_0 \to 0$ of long laser pulses, a single-value $\Delta\epsilon_{cv\mathbf{k}}$ is selected, which, however, corresponds to multiple $\mathbf{k}$ points and multiple values of $\Delta\epsilon_{cc'\mathbf{k}}$. We expect longer dephasing times for smaller detuning, a prediction which could be easily verified experimentally.

The analysis of the nonequilibrium dynamics has been carried out using the TD-IP approximation of the Kadanoff-Baym equations (3). The present results open the way to consider a number of extensions, like a detailed analysis of the relation between T_2' and $\{\omega_0, \Delta_0\}$ for a wide range of materials, and the introduction of terms beyond the TD-IP approximation. In particular the TD-IP approximation neglects the physics of the exciton. This is well justified here since the detuning is much bigger than the exciton binding energy in GaAs (≈ 10 meV). For future works, we plan to consider the role played by excitons when the difference between the pump energy and the optical gap is of the order of the excitonic binding energy.

Let us conclude by discussing how our results address one of the key questions in ultrafast demagnetization experiments: Where has the magnetization gone? In our case the magnetization is *still there*. The angular momentum oscillates back and forth, with different frequencies. However, it is distributed over an infinite number of degrees of freedom, and it is *not measurable anymore*. Letting the atoms be free to move, we would expect a periodic transfer of angular momentum between the electrons spin S_z and the atoms (or coherent phonons states). As for the electronic case, the coherent phonons would likely experience decoherence, and no macroscopic momentum would be detected experimentally beyond a few picoseconds.

ACKNOWLEDGMENTS

We acknowledge funding from Ministero dell'istruzione, dell'universitá e della ricerca (MIUR) (Italy), PRIN Grant No. 20173B72NB from the European Union, the project MaX Materials design at the eXascale H2020-EINFRA-2015-1 (Grant Agreement No. 824143), and the project Nanoscience Foundries and Fine Analysis-Europe H2020-INFRAIA-2014-2015 (Grant Agreement No. 654360).

[1] E. Beaurepaire, J.-C. Merle, A. Daunois, and J.-Y. Bigot, Ultrafast Spin Dynamics in Ferromagnetic Nickel, Phys. Rev. Lett. **76**, 4250 (1996).

[2] A. Kirilyuk, A. V. Kimel, and T. Rasing, Ultrafast optical manipulation of magnetic order, Rev. Mod. Phys. **82**, 2731 (2010).

[3] M. Wu, J. Jiang, and M. Weng, Spin dynamics in semiconductors, Phys. Rep. **493**, 61 (2010).

[4] I. Žutić, J. Fabian, and S. Das Sarma, Spintronics: Fundamentals and applications, Rev. Mod. Phys. **76**, 323 (2004).

[5] N. S. Averkiev and M. M. Glazov, Specific features of optical orientation and relaxation of electron spins in quantum wells with a large spin splitting, Semiconductors **42**, 958 (2008).

[6] F. Meier and B. Zakharchenya, *Optical Orientation*, Ed. by F. Meier and B. P. Zakharchenya (Elsevier, Amsterdam, 1984; Nauka, Leningrad, 1989).

[7] D. T. Pierce and F. Meier, Photoemission of spin-polarized electrons from GaAs, Phys. Rev. B **13**, 5484 (1976).

[8] S. Pfalz, R. Winkler, T. Nowitzki, D. Reuter, A. D. Wieck, D. Hägele, and M. Oestreich, Optical orientation of electron spins in GaAs quantum wells, Phys. Rev. B **71**, 165305 (2005).

[9] M. Dyakonov and V. I. Perel, *Optical Orientation* (Elsevier, Amsterdam, 1984), Chap. 2.

[10] F. Nastos, R. W. Newson, J. Hübner, H. M. van Driel, and J. E. Sipe, Terahertz emission from ultrafast optical orientation of spins in semiconductors: Experiment and theory, Phys. Rev. B **77**, 195202 (2008).

[11] J. Rioux and J. Sipe, Optical injection processes in semiconductors, Phys. E (Amsterdam, Neth.) **45**, 1 (2012).

[12] F. Nastos, J. Rioux, M. Strimas-Mackey, B. S. Mendoza, and J. E. Sipe, Full band structure LDA and $\mathbf{k}\cdot\mathbf{p}$ calculations of optical spin-injection, Phys. Rev. B **76**, 205113 (2007).

[13] T. T. Zhang, P. Barate, C. T. Nguyen, A. Balocchi, T. Amand, P. Renucci, H. Carrere, B. Urbaszek, and X. Marie, L-valley electron spin dynamics in GaAs, Phys. Rev. B **87**, 041201(R) (2013).

[14] N. Tancogne-Dejean, F. G. Eich, and A. Rubio, Time-dependent magnons from first principles, J. Chem. Theory Comput. **16**, 1007 (2020).

[15] J. M. Kikkawa, I. P. Smorchkova, N. Samarth, and D. D. Awschalom, Room-temperature spin memory in two-dimensional electron gases, Science **277**, 1284 (1997).

[16] J. M. Kikkawa and D. D. Awschalom, Resonant Spin Amplification in *n*-Type GaAs, Phys. Rev. Lett. **80**, 4313 (1998).

[17] K. Krieger, J. K. Dewhurst, P. Elliott, S. Sharma, and E. K. U. Gross, Laser-induced demagnetization at ultrashort time scales: Predictions of TDDFT, J. Chem. Theory Comput. **11**, 4870 (2015).

[18] V. Shokeen, M. Sanchez Piaia, J.-Y. Bigot, T. Müller, P. Elliott, J. K. Dewhurst, S. Sharma, and E. K. U. Gross, Spin Flips versus Spin Transport in Nonthermal Electrons Excited by Ultrashort Optical Pulses in Transition Metals, Phys. Rev. Lett. **119**, 107203 (2017).

[19] J. Simoni, M. Stamenova, and S. Sanvito, Ultrafast demagnetizing fields from first principles, Phys. Rev. B **95**, 024412 (2017).

[20] J. Shah, *Ultrafast Spectroscopy of Semiconductors and Semiconductor Nanostructures* (Springer, Berlin, 1996).

[21] C. Gardiner and P. Zoller, *Quantum Noise* (Springer, Berlin, 2004).

[22] M. W. Wu and C. Z. Ning, A novel mechanism for spin dephasing due to spin-conserving scatterings, Eur. Phys. J. B **18**, 373 (2000).

[23] M. W. Wu and H. Metiu, Kinetics of spin coherence of electrons in an undoped semiconductor quantum well, Phys. Rev. B **61**, 2945 (2000).

[24] M. Q. Weng and M. W. Wu, Spin dephasing in *n*-type GaAs quantum wells, Phys. Rev. B **68**, 075312 (2003).

[25] D. Stich, J. Zhou, T. Korn, R. Schulz, D. Schuh, W. Wegscheider, M. W. Wu, and C. Schüller, Effect of Initial Spin Polarization on Spin Dephasing and the Electron *g* Factor in a High-Mobility Two-Dimensional Electron System, Phys. Rev. Lett. **98**, 176401 (2007).

[26] C. P. Slichter, *Principles of Magnetic Resonance* (Springer, Berlin, 1990).

[27] C. F. Klingshirn, *Semiconductor Optics* (Springer, Berlin, 2012), Chaps. 23 and 27.

[28] A. Marini, C. Hogan, M. Grüning, and D. Varsano, yambo: An *ab initio* tool for excited state calculations, Comput. Phys. Commun. **180**, 1392 (2009).

[29] D. Sangalli, A. Ferretti, H. Miranda, C. Attaccalite, I. Marri, E. Cannuccia, P. Melo, M. Marsili, F. Paleari, A. Marrazzo, G. Prandini, P. Bonfà, M. O. Atambo, F. Affinito, M. Palummo, A. Molina-Sánchez, C. Hogan, M. Grüning, D. Varsano, and A. Marini, Many-body perturbation theory calculations using the yambo code, J. Phys.: Condens. Matter **31**, 325902 (2019).

[30] J. P. Perdew, K. Burke, and M. Ernzerhof, Generalized Gradient Approximation Made Simple, Phys. Rev. Lett. **77**, 3865 (1996).

[31] P. Giannozzi, S. Baroni, N. Bonini, M. Calandra, R. Car, C. Cavazzoni, D. Ceresoli, G. L. Chiarotti, M. Cococcioni, I. Dabo, A. D. Corso, S. de Gironcoli, S. Fabris, G. Fratesi, R. Gebauer, U. Gerstmann, C. Gougoussis, A. Kokalj, M. Lazzeri, L. Martin-Samos, N. Marzari, F. Mauri, R. Mazzarello, S. Paolini, A. Pasquarello, L. Paulatto, C. Sbraccia, S. Scandolo, G. Sclauzero, A. P. Seitsonen, A. Smogunov, P. Umari, and R. M. Wentzcovitch, QUANTUM ESPRESSO: A modular and open-source software project for quantum simulations of materials, J. Phys.: Condens. Matter **21**, 395502 (2009).

[32] P. Giannozzi, O. Andreussi, T. Brumme, O. Bunau, M. B. Nardelli, M. Calandra, R. Car, C. Cavazzoni, D. Ceresoli, M. Cococcioni, *et al.*, Advanced capabilities for materials modeling with QUANTUM ESPRESSO, J. Phys.: Condens. Matter **29**, 465901 (2017).

[33] Z. H. Levine and D. C. Allan, Linear Optical Response in Silicon and Germanium Including Self-Energy Effects, Phys. Rev. Lett. **63**, 1719 (1989).

[34] V. Fiorentini and A. Baldereschi, Dielectric scaling of the self-energy scissor operator in semiconductors and insulators, Phys. Rev. B **51**, 17196 (1995).

[35] K. A. Johnson and N. W. Ashcroft, Corrections to density-functional theory band gaps, Phys. Rev. B **58**, 15548 (1998).

[36] M. Gmitra and J. Fabian, First-principles studies of orbital and spin-orbit properties of GaAs, GaSb, InAs, and InSb zinc-blende and wurtzite semiconductors, Phys. Rev. B **94**, 165202 (2016).